Cellulose (2021) 28:153–174
https://doi.org/10.1007/s10570-020-03552-5

ORIGINAL RESEARCH

Exponential decay analysis: a flexible, robust, data-driven methodology for analyzing sorption kinetic data

Samuel V. Glass · Samuel L. Zelinka · Emil Engelund Thybring

Received: 23 April 2020 / Accepted: 22 October 2020 / Published online: 4 November 2020

Abstract The performance of cellulosic materials is intimately linked to their moisture content. Over the last century, many studies have been devoted to examining the moisture uptake in equilibrium with surrounding environmental conditions. However, with the adoption of automated sorption balances in laboratories worldwide, it has become increasingly popular to study the approach to equilibrium, i.e., sorption kinetics. Recording the moisture content change between two equilibrium states produces a wealth of data, which necessitates a robust methodology for analysis. In this study, we employ exponential decay analysis on sorption kinetic data obtained in a previous study for loblolly pine, holocellulose, office paper and microcrystalline cellulose. Unlike other methods that are constrained by a fixed number of fitting parameters or similar constraints, exponential decay analysis is a flexible, data-driven methodology for analyzing sorption kinetics. No physical meaning is assigned to the output from the analysis. However, the methodology yields robust results in relation to various measurement uncertainties. As a result, exponential decay analysis can provide a reliable description of the dominant time scales of sorption kinetics. Hereby, the methodology offers a new way to evaluate the suitability of theoretical models for describing sorption kinetics.

Keywords Sorption kinetics · Analysis methods · Moisture · Wood · Cellulose

Introduction

Water vapor sorption in cellulosic materials has been studied for over a century because of the marked effect water has on the physical properties of these materials (Barkas 1932; Glass et al. 2014; Pidgeon and Maass 1930; Sheppard and Newsome 1929, 1930; Thybring et al. 2018; Tiemann 1906; Urquhart 1929; Urquhart and Williams 1924; Volbehr 1896). Most of the studies in this area have focused on the moisture content of the material in equilibrium with constant climatic conditions in terms of temperature and relative humidity (RH), the so called, "sorption isotherm". With automated sorption balances (often referred to as "Dynamic Vapor Sorption" instruments

Electronic supplementary material The online version of this article (https://doi.org/10.1007/s10570-020-03552-5) contains supplementary material, which is available to authorized users.

S. V. Glass · S. L. Zelinka
Building and Fire Sciences, US Forest Service Forest Products Laboratory, Madison, WI, USA

E. E. Thybring (✉)
Department of Geosciences and Natural Resource Management, University of Copenhagen, Frederiksberg, Denmark
e-mail: eet@ign.ku.dk

or "DVS") becoming ever more commonplace in laboratories worldwide, detailed information on the moisture uptake in materials is now readily available. Not only does DVS yield information on equilibrium sorption behavior but also provides data on the approach to equilibrium, typically referred to as sorption kinetics. This has prompted several studies of the sorption kinetics, and theories have been developed to explain the experimental data (Kohler et al. 2003; Krabbenhøft and Damkilde 2004; Murr and Lackner 2018; Olek et al. 2005; Willems 2017). Many studies have claimed that sorption kinetics exhibit exponential behavior (Guo et al. 2017; Hill et al. 2010; Himmel and Mai 2016; Kohler et al. 2003; Simón et al. 2017; Zaihan et al. 2010), which is similar to a wide range of phenomena in nature such as first-order chemical reactions, radioactive decay, and the loss of coherence in the nuclear spins in LFNMR relaxometry (Istratov and Vyvenko 1999). As a result, the kinetics of sorption are often described by a sum of exponentials:

$$E = \frac{M(t) - M_0}{M_\infty - M_0} = 1 - \sum_{n=1}^{N} A_n \exp\left(-\frac{t}{\tau_n}\right) \quad (1)$$

where E (−) is the fractional change in moisture content at time t (s) in a sorption step between two equilibrium states, $M(t)$ (g g^{-1}) is the moisture content as a function of time, M_0 (g g^{-1}) is the initial moisture content at time $t = 0$, M_∞ (g g^{-1}) is the final equilibrium moisture content, N is the number of exponentials used to describe the sorption process, A_n is the nth pre-exponential coefficient, τ_n (s) is the nth characteristic time constant, and index n denotes the nth component of the sorption process. The parameter E varies from 0 to 1 in a complete sorption step, and is often used in the literature to compare changes in moisture content in specimens of different sizes and for different step changes in relative humidity (Christensen and Kelsey 1959; Wadsö 1993).

As shown in Table 1, the mathematical form in Eq. (1) is found for a range of empirical and theoretical models describing kinetics of sorption and other phenomena such as chemical reactions. All of these models have been algebraically re-arranged to the same mathematical form as Eq. (1) (Thybring et al. 2019b). The Fickian models are used to describe the sorption process by Fickian diffusion of water molecules into or out of the material. Depending on the surface boundary conditions (constant, changing over time, convective) the mathematical expressions of Fickian models differ. However, it can be seen that the pre-exponential coefficients and characteristic time constants are both given by infinite series that rapidly decrease in magnitude with increasing n. The Berens–Hopfenberg (Berens and Hopfenberg 1978) model incorporates the effect of stress relaxation on sorption in polymeric materials by adding exponential components describing relaxation to a Fickian diffusion model. In Table 1, the latter is described for a planar geometry. The simplest and one of the most widely applied models in Table 1 is the empirical Lagergren (1898) model, which describes what is called pseudo-first order kinetics. The model is mathematically similar to the Linear Driving Force (LDF) model (Glueckauf and Coates 1947; Sircar 1983) and the film diffusion mass transfer rate equation (Boyd et al. 1947), although the constituent parameters differ between the three models. The two latter are both derived from physical frameworks. Building on top of the LDF model, Sircar (1983) coupled heat and mass transfer in chemical reactions, while the mathematically equivalent thermally limited moisture transport (TLMT) model was developed by Willems (2017) to explain coupled heat and moisture transport involved in sorption kinetics. These are mathematically equivalent to other theoretical models coupling heat and moisture transport (Chihara et al. 1976; Lee and Ruthven 1979; Wang et al. 1996). Finally, the parallel exponential kinetics (PEK) model was developed by Kohler et al. (2003) to describe sorption in cellulosic materials. As seen from Table 1, the PEK model is similar to the Sircar and TLMT models as well as the widely applied double exponential model by Wilczak and Keinath (1993).

Currently, the most popular model for describing sorption kinetics in cellulosic materials is the PEK model, but we have recently shown that it mischaracterizes sorption kinetics to equilibrium for wood and microcrystalline cellulose, see (Thybring et al. 2019a,b) and references cited in these articles. The problem with the PEK model is that the sum of two exponentials is unable to mathematically capture the actual shape of the sorption curves because in nearly all cases more than two exponential components are needed to describe the sorption kinetic data (Thybring et al. 2019a). Thus, forcing two exponentials onto the data does not provide reliable results, and the model

Table 1 Similarity in mathematical form between empirical and theoretical models describing the kinetics of sorption and chemical reactions. The Berens-Hopfenberg model is a sum of contributions from Fickian diffusion (relative weight, φ_D) and relaxation in polymeric materials (relative weight, φ_R). The Fickian models are given for a planar geometry (Crank 1975) with Fickian1 describing a constant surface condition equal to the equilibrium concentration ($c_{surf} = c_\infty$), Fickian2 describing a surface concentration approaching the equilibrium concentration over time ($c_{surf} = c_\infty$ [1-exp(-βt)]), and Fickian3 describing the convective surface condition (flux at surface, $F_{surf} = -\alpha [c_{surf} - c_0]/D$ where c_0 is the initial concentration). The Lagergren (1898) model describes chemical pseudo-first order reaction kinetics. The Sircar (1983) model couples mass and heat transfer in chemical reactions, while the TLMT model is developed specifically for sorption kinetics (Willems 2017). TLMT = thermally limited moisture transport, PEK = parallel exponential kinetics

Model	Re-arranged form	Parameters of Eq. (1)
Berens–Hopfenberg	$E = 1 - \varphi_R \sum_{i=1}^{k} K_i \exp[-\beta_i t] - \varphi_D \sum_{n=k}^{\infty} \frac{8}{(2n-2k+1)^2\pi^2} \exp\left[\frac{-(2n-2k+1)^2\pi^2}{4L^2} Dt\right]$	$N = \infty$ $A_i = \varphi_R K_i,\ 0 < i \le k$ $A_n = \varphi_D \frac{8}{(2n-1)^2\pi^2},\ n > k$ $\tau_i = \frac{1}{\beta_i},\ 0 < i \le k$ $\tau_n = \frac{4L^2}{D(2n-3)^2\pi^2},\ n > k$
Fickian1	$E = 1 - \sum_{n=1}^{\infty} \frac{8}{(2n-1)^2\pi^2} \exp\left[\frac{-(2n-1)^2\pi^2}{4L^2} Dt\right]$	$N = \infty$ $A_n = \frac{8}{(2n-1)^2\pi^2}$ $\tau_n = \frac{4L^2}{D(2n-1)^2\pi^2}$
Fickian2	$E = 1 - \sqrt{\frac{D}{\beta L^2}} tan\left(\sqrt{\frac{\beta L^2}{D}}\right) \exp(-\beta t) - \sum_{n=2}^{\infty} \frac{8}{(2n-3)^2\pi^2\left[1-(2n-3)^2\left(\frac{D\pi^2}{4\beta L^2}\right)\right]} \exp\left[\frac{-(2n-3)^2\pi^2}{4L^2} Dt\right]$	$N = \infty$ $A_1 = \sqrt{\frac{D}{\beta L^2}} tan\left(\sqrt{\frac{\beta L^2}{D}}\right)$ $A_n = \frac{8}{(2n-3)^2\pi^2\left[1-(2n-3)^2\left(\frac{D\pi^2}{4\beta L^2}\right)\right]},\ n > 1$ $\tau_1 = \frac{1}{\beta}$ $\tau_n = \frac{4L^2}{D(2n-3)^2\pi^2},\ n > 1$
Fickian3	$E = 1 - \sum_{n=1}^{\infty} \frac{2\lambda^2}{\beta_n^2\left(\beta_n^2+\lambda^2+\lambda\right)} \exp\left[\frac{-\beta_n^2}{L^2} Dt\right]$	$N = \infty$ $A_n = \frac{2\lambda^2}{\beta_n^2\left(\beta_n^2+\lambda^2+\lambda\right)}$ $\tau_n = \frac{L^2}{D\beta_n^2}$ β_n are the positive roots of $\beta tan(\beta) = \lambda = \frac{\alpha L}{D}$
Lagergren	$E = 1 - \exp[-k_1 t]$	$N = 1$ $A_1 = 1$ $\tau_1 = \frac{1}{k_1}$
PEK	$E = 1 - \sum_{n=1}^{2} \frac{\Delta M_n}{M_\infty - M_0} \exp\left(\frac{-t}{\tau_n}\right)$	$N = 2$ $A_n = \left\{\frac{\Delta M_1}{M_\infty - M_0}, \frac{\Delta M_2}{M_\infty - M_0}\right\}$ $\tau_n = \{\tau_1, \tau_2\}$
Sircar	$E = 1 - \frac{\beta\alpha^2}{\beta\alpha^2 - 1} \exp\left[-\frac{k\alpha - k}{\alpha} t\right] - \frac{1}{1-\beta\alpha^2} \exp[-k(1-\alpha\beta)t]$	$N = 2$ $A_n = \left\{\frac{\beta\alpha^2}{\beta\alpha^2-1}, \frac{1}{1-\beta\alpha^2}\right\}$ $\tau_n = \left\{\frac{\alpha}{k\alpha-k}, \frac{1}{k(1-\alpha\beta)}\right\}$
TLMT	$E = 1 - \left[\frac{-1-b_2}{b_1-b_2} exp\left(\frac{-t}{\tau_1}\right) + \frac{1+b_1}{b_1-b_2} exp\left(\frac{-t}{\tau_2}\right)\right]$	$N = 2$ $A_n = \left\{\frac{-1-b_2}{b_1-b_2}, \frac{1+b_1}{b_1-b_2}\right\}$ $\tau_n = \{\tau_1, \tau_2\}$

parameters cannot be related to physically meaningful properties. This problem will also apply to the Sircar, TLMT and other mathematically equivalent models if they were fit to the same sorption kinetic data. Forcing a single exponential, e.g. the Lagergren model or similar, to fit such data would also lead to unreliable results. However, it should be noted that the goodness of fit as described by the R^2 parameter can be close to unity even if the fit of one of the previously mentioned models does not capture the shape of the sorption curve. This has for instance been demonstrated by fits of the PEK model to experimental sorption data (Jalaludin et al. 2010; Xie et al. 2011).

Therefore, another approach is needed to evaluate whether a given model equivalent to Eq. (1) can reliably characterize sorption kinetic data. The models given in Table 1 are all contained in this equation; however, they are constrained either in the relation between individual pre-exponential coefficients and time constants or in the number of exponentials. As an alternative to fitting one or several of these models, Thybring et al. (2019a) suggested a data-driven approach known as exponential decay analysis.

As opposed to previous methods, where a physical or structural model is applied to fit the data, this method does not impose constraints on the fitted exponentials and is a flexible methodology which identifies the different timescales of sorption kinetics. A data-driven approach is useful because it has already been shown that structural models, such as the PEK model, can have very high R^2 values even though they do not contain the correct number of time constants (Thybring 2019a). A data-driven approach can serve as a basis to evaluate any model with an exponential structure, such as those in Table 1. Importantly, each of these models has a "fingerprint" of time constants and relative weights based on its mathematical form in Table 1. The model fingerprint can be compared with the fingerprint of the data determined by exponential decay analysis; for instance, if only two peaks are observed in the data, a Fickian model would not be appropriate. In summary, exponential decay analysis identifies the relevant timescales of the sorption process and is useful for testing physical or empirical models that have an exponential structure. Models that have other functional forms are not considered further in this work. While exponential decay analysis is useful, it does not constitute validation, which would involve testing model predictions under different experimental conditions and independently verifying the model parameters.

In this paper we employ exponential decay analysis for an in-depth investigation of the sorption kinetic data of the four cellulosic materials described by Glass et al. (2018). The analyses are performed with multi-exponential decay analysis (MEDEA) and discrete exponential fitting (DEXFIT), both of which are routinely used for analyzing low-field nuclear magnetic resonance (LFNMR) relaxometry data where agreement has been found between the two techniques (Araujo et al. 1992; Beck et al. 2018; Fredriksson and Thygesen 2017). MEDEA was previously used in Thybring et al. (2019a) on sorption kinetic data for loblolly pine and microcrystalline cellulose. This study extends the analysis to four different cellulosic materials, adds discrete exponential fitting, investigates the influence of MEDEA parameters, and evaluates the robustness of the analysis methods under various sources of experimental uncertainty. The results show that sorption kinetic data can be fit with a finite sum of exponential functions, and illustrate the value of the methodology for analyzing sorption kinetic data.

Materials and methods

Experimental sorption kinetic data

Four different cellulosic materials were examined: loblolly pine (*Pinus taeda*), holocellulose extracted from loblolly pine, microcrystalline cellulose (MCC), and office paper. These materials and the experimental details are described further in prior work (Glass et al. 2018). An automated sorption balance (IGAsorp gravimetric vapor sorption analyzer, Hiden Isochema, Warrington, UK) was used to collect sorption kinetic data at 25 °C of specimens with a mass around 20 mg. This instrument continuously monitors the mass of a specimen by a microbalance with a resolution of 0.1 μg. The specimen is placed in a stainless-steel basket suspended from the balance inside a thermally controlled chamber. In this, the RH around the specimen is controlled by continuously purging with a stream of moistened nitrogen gas with a flow of 250 mL min^{-1}. The humidity of the nitrogen gas is controlled by tuning the mixture of two gas streams: a dry and a vapor-saturated one. The sorption kinetic

measurements at a given RH were continued until the observed mass change was less than the slight fluctuations in observed mass of an inert sample over 24 h as a result of random noise, vibration, and instrument drift. For this instrument, the inherent mass stability was in previous work determined as at most 2 µg over a 24 h period (Glass et al. 2018).

In our prior work on exponential decay analysis (Thybring et al. 2019a), the raw sorption kinetic data were adjusted prior to exponential decay analysis by removing data points during the first minute of data collection after the instrument initiated the change in relative humidity. This was done because the instrument requires a certain amount of time to reach the new RH level and because we were comparing results with other studies that used this adjustment (see Thybring et al. 2019a) prior to fitting the PEK model. In this study, however, no such time adjustment was made to the data, and no data points were removed.

Exponential decay analysis

The sorption kinetic data were analyzed by two methods that we refer to as discrete exponential fitting (DEXFIT) and multi-exponential decay analysis (MEDEA). These methods are routinely used for analyzing LFNMR relaxometry data (Araujo et al. 1992; Beck et al. 2018; Fredriksson and Thygesen 2017), which consists of a signal that decays at decreasing rate over time, going from ~ 100% initially to 0% at the end of the measurement time. In exponential decay analysis, the characteristic time constant(s) and pre-exponential coefficient(s) are used as fitting parameters to minimize the residual error between the sum of one or more exponential function(s) and experimental data. The corresponding fitting parameters are used to characterize a given dataset.

In order to perform DEXFIT and MEDEA on the sorption kinetic data, these had to be converted to a format similar to that of LFNMR relaxometry data. Each sorption step between two levels of RH saw the moisture content change from the initial value (M_0) to a final moisture content (M_∞) in equilibrium with the new RH conditions. The kinetic data were first converted to fractional moisture content change over time, E, as described by Eq. (1). Since moisture content is the mass of water in the sample normalized by the dry mass, E was calculated directly from the recorded masses. The algorithm used to analyze the sorption kinetic data requires that a time series changes from around 1–0 over the sorption step. For this reason, the moisture content changes were evaluated from the parameter $1 - E$. This "decay function" $1 - E$ is expressed hereafter as a percentage. Figure 1 illustrates the conversion of sorption kinetic data from mass to moisture content to $1 - E$, all as a function of time. It is important to point out that the conversion to $1 - E$ requires the specimen to reach moisture equilibrium at the end of the sorption step. For the datasets in this study, as described above, equilibrium was operationally defined as a change in

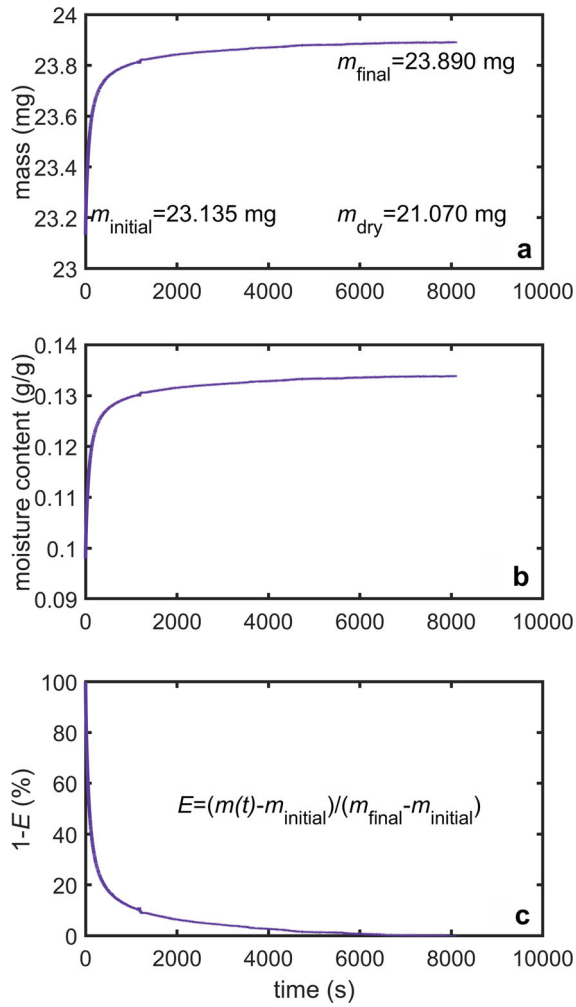

Fig. 1 Conversion of recorded mass over time into $1 - E$ for loblolly pine in the sorption step 70–80% RH: **a** Recorded specimen mass, **b** calculated moisture content (in grams of moisture per gram of dry material), and **c** normalized moisture content change $1 - E$

specimen mass less than the inherent mass stability of the sorption balance (Glass et al. 2018). Sorption should therefore not be interrupted by a commonly-used stop criterion, e.g. a less stringent mass stability criterion, since this results in an erroneous equilibrium mass at the end of the time series (Glass et al. 2017, 2018), which will affect the subsequent analysis.

DEXFIT

DEXFIT was performed by use of the "expfit" function (release version 1.5) in the MATLAB toolbox developed for analysis of LFNMR relaxometry data by Pedersen, Bro and Engelsen (Engelsen and Bro 2003; Pedersen et al. 2002). This function fits the data with the sum of a selected number of exponential components, which in this study was chosen to be from 1 to 7 for all sorption steps. The algorithm does not require initial estimates of the fitting parameters.

When the number of fitted exponentials increases, the algorithm at some point will produce nonsensical outputs. This will show up as pairs of exponentials with very closely spaced time constants and large pre-exponential coefficients (magnitude greater than 100) that balance each other out, i.e. one negative and one positive coefficient. The optimum number of components needed to adequately describe the sorption kinetic data was therefore selected as the maximum number of exponentials with sensible pre-exponential components.

MEDEA

MEDEA was performed by fitting a large number of exponential components with logarithmically spaced characteristic time constants to the sorption kinetic data. The range of time constants was chosen as the range between the first recorded data point at $t > 0$ and the last recorded data point. This method produces a smooth spectrum of amplitude versus time, from which the number of exponential components needed to describe the data is seen from the number of peaks appearing in the spectrum. The characteristic time constants of the components are directly seen from the location of the peaks on the abscissa and the corresponding pre-exponential coefficients can be derived from the sum of pre-exponential coefficients designating the given peak. MEDEA uses the non-negative least squares (NNLS) algorithm by Lawson and Hanson (1974) for minimizing the following statistic:

$$\chi^2 = \sum_{i=1}^{m}\left((1-E_i) - \sum_{n=1}^{N} A_n \mathrm{e}^{-t_i/\tau_n}\right)^2 + \frac{1}{\alpha}\sum_{n=1}^{N-2}(2A_{n+1} - A_n - A_{n+2})^2 \quad (2)$$

where m is the number of data points in the time series, $(1 - E_i)$ and t_i are the experimental signal and time of the ith data point, respectively, N is the number of exponential components fitted to the data, A_n is the amplitude (pre-exponential coefficient) of the nth component, τ_n is the characteristic time constant associated with the nth component, and α is a regularization parameter that controls the smoothness of the spectrum, i.e., the difference between adjacent pre-exponential coefficients A_n. These coefficients are constrained to non-negative values. The first summation in Eq. (2) corresponds to the sum of squared residuals between experimental data and the MEDEA fit, while the second summation imposes smoothness by penalizing abrupt changes between neighboring pre-exponential coefficients. In this study, $N = 200$ exponential components were fitted to the sorption kinetic data by the MEDEA algorithm after selecting an appropriate regularization parameter, $\alpha = 10^9$; see further discussion of these parameters in the Results and Discussion.

There is a limit to the number of exponential components that can be resolved with DEXFIT and MEDEA from the experimental data (Istratov and Vyvenko 1999). This resolution limit is given as a minimum spacing required between the time constants of adjacent exponential components. The resolution limit depends on the signal-to-noise ratio and is calculated by the ratio of the time constants as (Bertero et al. 1982)

$$\delta = \frac{\tau_i}{\tau_{i+1}} = exp\left[\frac{\pi^2}{arcosh\left(\pi(SNR)^2\right)}\right] \quad (3)$$

where δ (-) is the resolution limit, i.e. minimum spacing between the two neighboring time constants, τ_i and τ_{i+1}, where $\tau_i > \tau_{i+1}$, and SNR is the signal-to-noise ratio. The resolution limit constrains the amount of information that can be extracted from the data, and attempts to find time constants closer than the limit is

bound to produce unreliable results (McWhirter and Pike 1978; Ostrowsky et al. 1981). If the relaxation domain is known, i.e. the time range over which the exponential decay occurs, then the number of resolvable exponential components can be calculated as (Bertero et al. 1982)

$$N_{\max} = \frac{ln\left(\frac{b_0}{a_0}\right)}{ln(\delta)} \quad (4)$$

where b_0/a_0 is the ratio of the last to first time point in the relaxation range, and $N_{\max}$ is the maximum number of resolvable exponential components rounded down.

Besides investigating the sorption kinetic data, this study also examined the influence of the MEDEA parameters (number of exponentials and regularization parameter) on the shape of the spectra. Furthermore, we explored the effects of various uncertainties on the derived fitting parameters from DEXFIT and MEDEA, including the inherent instrument mass stability, i.e., long-term instrument drift, random noise, negative data, erratic mass instability, and inadequate equilibrium at the end of sorption.

Results and discussion

The results of the MEDEA and DEXFIT fitting routines are illustrated by Fig. 2. The mass data were transformed to $1 - E$, and these data were then fit with the MEDEA and DEXFIT routines for each relative humidity step examined. The top row of Fig. 2 illustrates the $1 - E$ fit for MEDEA and DEXFIT for a 70–80% RH step for loblolly pine. For illustrative purposes, the fits were transformed to mass as a function of time and the residuals are plotted in the middle two rows of Fig. 2. It can be seen that both exponential decay analysis methods fit the data extremely well and had similar residuals. Finally, the spectra of amplitudes as a function of time from each method are illustrated in the final row of Fig. 2. In the case of DEXFIT, the spectrum represents the relative contributions of each discrete exponential component, while in the case of MEDEA the spectrum is a series of peaks that can be described by the peak times and relative peak areas. These kinetic fingerprints are presented for all RH steps examined in Figs. 3 and 4 and Tables 2 and 3.

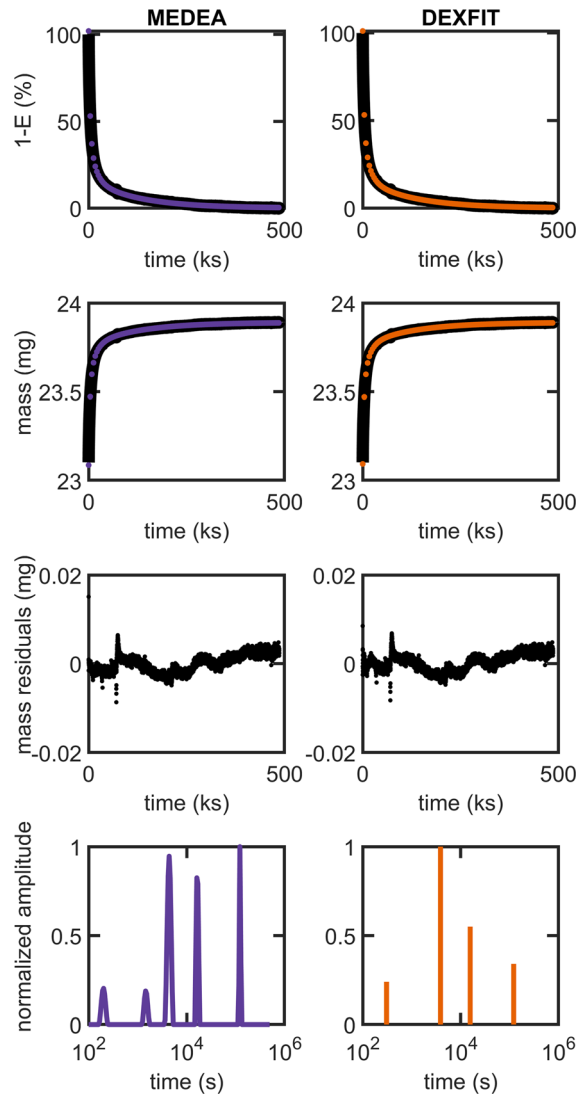

Fig. 2 Fitting of exponentials by MEDEA (left column) and DEXFIT (right column) to data for loblolly pine in the sorption step 70–80% RH. Top row: data presented as $(1 - E)$ along with fits. Second row: data presented as mass. Third row: mass residuals. Bottom row: amplitude as a function of time for the exponential fits

The spectra fit to sorption kinetic data for all four cellulosic materials and all sorption steps are illustrated in Fig. 3 and Table 2 for absorption and in Fig. 4 and Table 3 for desorption. In general, it is seen that the derived fitting parameters from DEXFIT and MEDEA agree reasonably well. In Figs. 3, 4 the number of exponentials and their characteristic time constants found by the two analysis methods can be seen, and from Tables 2 and 3 the relative weights of

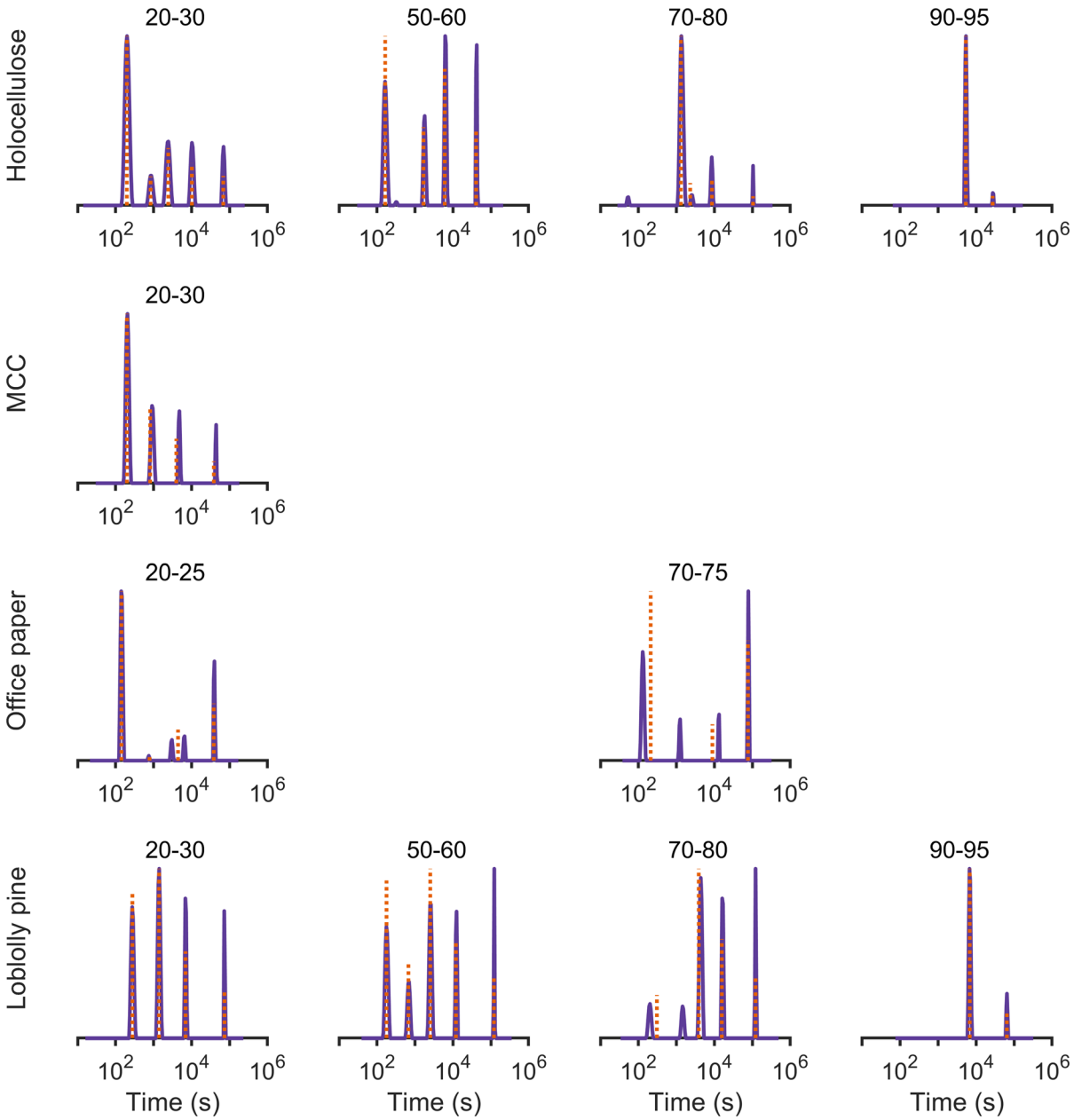

Fig. 3 MEDEA spectra (solid curves) and DEXFIT spectra (discrete dotted lines) for all absorption steps examined. Ordinate is normalized amplitude (labels omitted for clarity)

the exponentials can be seen. Overall, the same number of exponential components needed to adequately describe the mathematical form of the sorption curve was found in 11 out of 21 sorption steps. For the remaining 10 cases, MEDEA found one more exponential component than DEXFIT in eight sorption steps, and two more components in two steps. As seen in Figs. 3 and 4, in the cases where the number of exponentials is larger for MEDEA than DEXFIT, the previous method usually finds two closely spaced peaks, whereas DEXFIT only finds one exponential with a time constant that appears between the two closely spaced exponentials found by MEDEA. Moreover, the relative weights found with DEXFIT

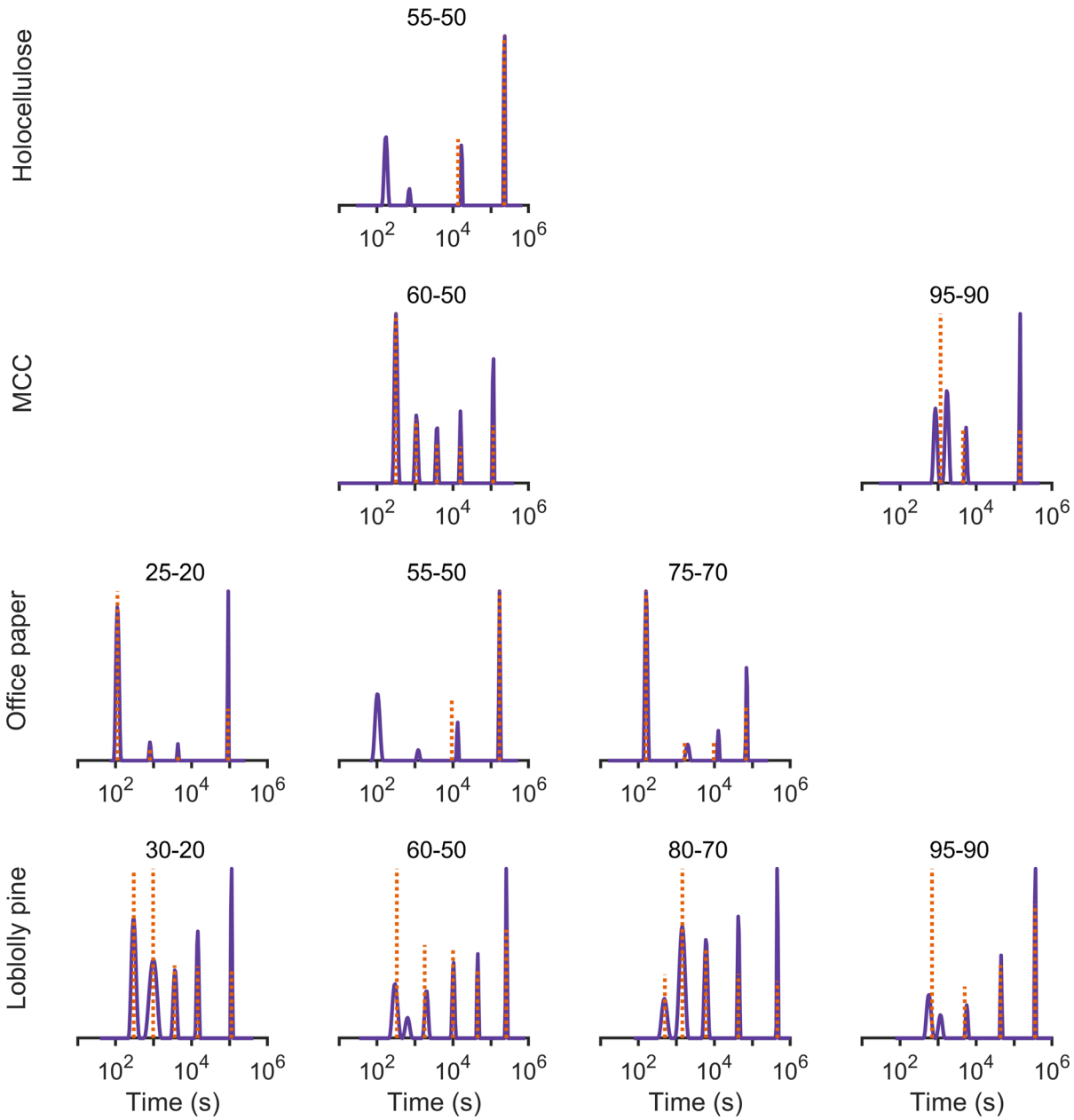

Fig. 4 MEDEA spectra (solid curves) and DEXFIT spectra (discrete dotted lines) for all desorption steps examined. Ordinate is normalized amplitude (labels omitted for clarity)

and MEDEA and shown in Tables 2 and 3 are seen to be very similar. For those cases where one or two more exponentials are found with MEDEA, the overall pattern in the distribution of the relative weights is reproduced by DEXFIT. The close correspondence between the fitting parameters found by the two methodologies, despite their different approaches to analyze the data, gives confidence about the robustness of the results and that these are descriptive of the mathematical form of the sorption kinetic data.

Table 2 MEDEA and DEXFIT parameters for all absorption steps

Material, RH step	MEDEA			DEXFIT		
	Peak	Peak time	Relative weight (%)	n	τ_n	Relative weight (%)
Holocellulose	1	199 s	52.3	1	198 s	51.7
20–30% RH	2	831 s	7.8	2	834 s	8.9
	3	2.45 ks	18.0	3	2.43 ks	17.5
	4	10.2 ks	13.0	4	10.2 ks	12.9
	5	69.6 ks	8.9	5	68.4 ks	9.0
Holocellulose	1	163 s	36.6	1	164 s	36.9
50–60% RH	2	317 s	0.6			
	3	1.80 ks	18.0	2	1.67 ks	17.1
	4	6.25 ks	28.9	3	6.07 ks	29.7
	5	42.3 ks	15.9	4	40.7 ks	16.3
Holocellulose	1	54 s	2.2	1	1.31 ks	74.7
70–80% RH	2	1.35 ks	79.2			
	3	2.49 ks	3.2	2	2.31 ks	9.9
	4	8.52 ks	11.4	3	8.62 ks	11.3
	5	104 ks	4.0	4	104 ks	4.1
Holocellulose	1	5.45 ks	94.8	1	5.41 ks	94.7
90–95% RH	2	27.6 ks	5.2	2	27.4 ks	5.3
Microcrystalline	1	205 s	56.1	1	198 s	54.3
cellulose	2	908 s	24.5	2	812 s	24.4
20–30% RH	3	4.78 ks	13.1	3	3.96 ks	14.3
	4	44.4 ks	6.3	4	38.5 ks	7.0
Office paper	1	140 s	64.8	1	142 s	64.5
20–25% RH	2	748 s	1.0	2	783 s	2.0
	3	3.04 ks	6.3	3	4.40 ks	11.8
	4	6.55 ks	6.9			
	5	40.0 ks	21.0	4	38.4 ks	21.7
Office paper	1	130 s	47.3	1	210 s	52.0
70–75% RH	2	1.26 ks	10.6	2	8.85 ks	11.2
	3	13.3 ks	8.7			
	4	78.3 ks	33.4	3	76.6 ks	36.8
Loblolly pine	1	273 s	32.2	1	276 s	32.2
20–30% RH	2	1.40 ks	37.9	2	1.39 ks	37.8
	3	6.86 ks	19.3	3	6.95 ks	19.4
	4	72.5 ks	10.6	4	73.4 ks	10.6

Table 2 continued

Material, RH step	MEDEA			DEXFIT		
	Peak	Peak time	Relative weight (%)	n	τ_n	Relative weight (%)
Loblolly pine	1	176 s	28.3	1	178 s	28.2
50–60% RH	2	696 s	13.4	2	671 s	13.3
	3	2.62 ks	30.4	3	2.52 ks	30.3
	4	12.4 ks	17.1	4	12.0 ks	17.3
	5	122 ks	10.8	5	120 ks	10.9
Loblolly pine	1	202 s	9.6	1	307 s	11.6
70–80% RH	2	1.45 ks	7.7			
	3	4.39 ks	42.2	2	3.88 ks	45.4
	4	16.1 ks	24.3	3	15.7 ks	26.6
	5	121 ks	16.2	4	121 ks	16.4
Loblolly pine	1	6.75 ks	86.0	1	6.86 ks	85.9
90–95% RH	2	65.0 ks	14.0	2	64.8 ks	14.1

Influence of MEDEA parameters

Number of exponentials

The resolvable number of exponentials in each dataset is found by Eq. (4) and is given by the signal-to-noise ratio and relaxation domain, i.e. the time range. For the sorption kinetic data of this study, this maximum number of resolvable exponentials was between 10–18, see Table 4. Nonetheless, the number of exponentials selected in MEDEA was set to 200. This was done to guarantee that the relaxation domain was properly sampled with MEDEA by allowing 10–20 times more exponentials to be fitted to the data than could be resolved based on the signal-to-noise ratio. Afterwards, the spacing of the time constants associated with the peaks found by MEDEA was calculated and compared to the resolution limit given by Eq. (3).

Regularization parameter α

The regularization parameter, α, controls the smoothness of the spectrum of exponentials found by MEDEA. At low values of α, the spectrum is smooth and individual peaks cannot be resolved even if their spacing exceeds the resolution limit. In this situation, information contained in the data is lost due to over-smoothing. Conversely, at high values of α, the spectrum becomes spiky and there is a risk of artifacts in the form of peaks designated by single, non-zero (but often small) pre-exponential coefficients. Finding the right value of α is not a trivial task (Istratov and Vyvenko 1999), but a common method is to select a value close to the threshold between the smoothed and spiky domains. This threshold is illustrated in Fig. 5a by plotting the normalized χ^2 against α. Figure 5b shows the corresponding spectra of pre-exponential coefficients for five of the α-values highlighted in Fig. 5a. The change from a smooth to a spiky spectrum is clearly visible. For the rest of the study, a value of $\alpha = 10^9$ is selected for MEDEA, which is on the upper side of the threshold seen in Fig. 5a. The introduction of artifacts as a result of noise with a much larger α is shown in Fig. S1 of the *Supplementary Material*.

Uncertainties involved in exponential decay analysis

The uncertainties involved in the analysis with DEXFIT and MEDEA were evaluated based upon sorption data of loblolly pine and holocellulose.

Instrument drift

The effect of instrument drift on the DEXFIT and MEDEA results was analyzed by adding or subtracting a drift of 2 μg day^{-1} to the mass curves of the sorption steps 20–30, 30–20, 70–80, and 80–70% RH of

Table 3 MEDEA and DEXFIT parameters for all desorption steps

Material, RH step	MEDEA			DEXFIT		
	Peak	Peak time	Relative weight (%)	n	τ_n	Relative weight (%)
Holocellulose	1	174 s	40.2	1	13.6 ks	28.2
55–50% RH	2	717 s	6.0			
	3	16.6 ks	13.6			
	4	232 ks	40.2	2	224 ks	71.8
Microcrystalline	1	316 s	46.2	1	313 s	45.9
cellulose	2	1.08 ks	17.0	2	1.08 ks	17.3
60–50% RH	3	3.89 ks	11.2	3	3.78 ks	11.2
	4	15.7 ks	9.9	4	15.7 ks	9.9
	5	117 ks	15.7	5	114 ks	14.7
Microcrystalline	1	858 s	30.0	1	1.17 ks	60.8
cellulose	2	1.70 ks	37.8			
95–90% RH	3	5.50 ks	12.9	2	4.58 ks	19.7
	4	145 ks	19.3	3	143 ks	19.5
Office paper	1	110 s	70.7	1	112 s	70.6
25–20% RH	2	801 s	4.8	2	800 s	4.8
	3	4.36 ks	3.0	3	4.39 ks	3.0
	4	92.6 ks	21.5	4	91.4 ks	21.6
Office paper	1	101 s	51.4	1	9.30 ks	26.5
55–50% RH	2	1.21 ks	4.4			
	3	13.3 ks	9.6			
	4	168 ks	34.6	2	167 ks	73.5
Office paper	1	158 s	65.3	1	159 s	65.0
75–70% RH	2	1.99 ks	8.0	2	1.65 ks	7.4
	3	12.7 ks	7.1	3	9.60 ks	7.1
	4	69.8 ks	19.6	4	67.7 ks	20.5
Loblolly pine	1	290 s	30.0	1	301 s	30.6
30–20% RH	2	975 s	32.0	2	972 s	30.7
	3	3.60 ks	12.7	3	3.57 ks	13.2
	4	14.6 ks	12.9	4	14.4 ks	13.0
	5	114 ks	12.4	5	112 ks	12.5
Loblolly pine	1	300 s	26.5	1	333 s	32.0
60–50% RH	2	641 s	8.3			
	3	2.06 ks	15.4	2	1.80 ks	17.6
	4	10.4 ks	16.9	3	10.0 ks	17.2
	5	45.2 ks	12.5	4	44.3 ks	12.7
	6	253 ks	20.4	5	255 ks	20.5

Table 3 continued

Material, RH step	MEDEA			DEXFIT		
	Peak	Peak time	Relative weight (%)	n	τ_n	Relative weight (%)
Loblolly pine	1	485 s	13.2	1	497 s	14.3
80–70% RH	2	1.43 ks	39.3	2	1.44 ks	38.0
	3	5.94 ks	20.3	3	5.98 ks	20.4
	4	42.4 ks	14.4	4	42.8 ks	14.4
	5	448 ks	12.8	5	454 ks	12.9
Loblolly pine	1	583 s	28.7	1	699 s	39.5
95–90% RH	2	1.15 ks	12.9			
	3	5.69 ks	10.6	2	5.06 ks	12.1
	4	45.8 ks	16.9	3	44.2 ks	17.1
	5	368 ks	30.9	4	357 ks	31.3

Table 4 Resolution limit (δ) of exponential decay analysis calculated from Eq. (3) for the various sorption steps based on the signal-to-noise ratio (SNR), the relaxation domain (b_0/a_0) defined by the ratio of the last (b_0) to first time point (a_0), and the maximum number of exponentials (N_{max}) that can be resolved in the relaxation domain as found by Eq. (4)

Material	RH step (%)	SNR	δ	b_0/a_0	N_{max}
Holocellulose	20–30	1075	1.9	17,048	15
	50–60	1510	1.8	6777	14
	70–80	2895	1.7	11,885	16
	90–95	1482	1.8	2575	13
	55–50	785	1.9	23,490	15
Microcrystalline cellulose	20–30	1543	1.8	5685	14
	60–50	1822	1.8	16,470	16
	95–90	1454	1.8	65,092	18
Office paper	20–25	196	2.2	7624	11
	70–75	418	2.0	8266	12
	25–20	203	2.2	15,307	12
	55–50	281	2.1	8058	11
	75–70	216	2.2	3695	10
Loblolly pine	20–30	1123	1.9	13,578	15
	50–60	471	2.0	8545	12
	70–80	1438	1.8	14,202	15
	90–95	2025	1.8	4160	14
	95–90	830	1.9	15,402	14
	80–70	2646	1.8	17,520	17
	60–50	1425	1.8	23,252	16
	30–20	1858	1.8	10,674	15

loblolly pine. This selection of sorption steps covers both absorption and desorption in the low and high moisture content regime. This instrument drift corresponds with the one experimentally determined for the utilized sorption balance loaded with an inert sample (Glass et al. 2018). The instrument was not found to drift more prominently in one direction. The results show an instrument drift of this magnitude typically had only a slight effect on the obtained fitting parameters with DEXFIT and MEDEA, but in some cases changed the number of components, as exemplified by Fig. 6 and seen in the *Supplementary Material* (Figs. S2–S4 and Tables S1–S2). However, in most cases the amplitude of the peaks changes

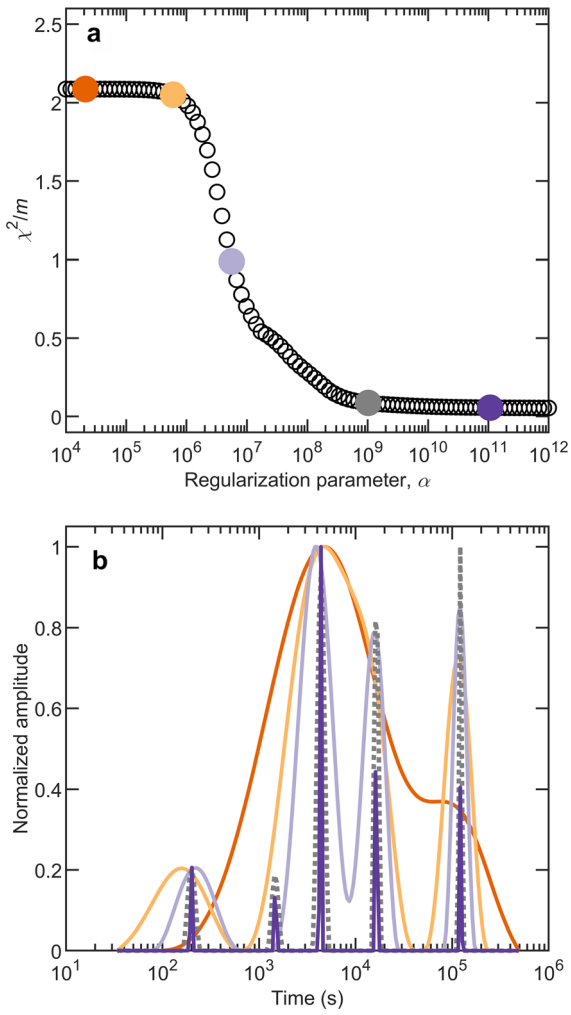

Fig. 5 Effect of the regularization parameter α on MEDEA spectra for moisture absorption in loblolly pine from 70 to 80% RH: **a** χ^2 normalized by the number of time points as a function of α; **b** amplitude normalized by the peak amplitude for each value of α. The number of exponential components N in all cases is 200

slightly in a systematic way. For absorption, an upward drift put more weight on the peaks with longer relaxation time whereas a downward drift put more weight on the peaks with shorter relaxation times. The opposite trends were seen for samples in desorption. This pattern is logical when comparing the $1 - E$ curves in absorption and desorption with added drift. The most pronounced shift in relaxation times is seen for the exponential component with the longest relaxation time. This is expected since the added constant drift is closest in magnitude to the observed rate of mass change towards the end of the sorption step.

Instrument random noise

Instrument random noise was characterized using the same data for an inert sample mentioned previously in regard to instrument drift. Analysis of the deviations from the mean mass over a series of 1 h time windows yielded a distribution that was close to a Gaussian (normal) distribution with a standard deviation of 0.9 µg. The effect of random noise from the instrument on the MEDEA results was analyzed by adding a Gaussian distributed noise with a standard deviation of 1 µg (and mean of 0 µg) to the sorption steps 20–30% and 70–80% RH in loblolly pine to cover both the low and high moisture content regime. It should be noted that this exaggerates the effect because noise is added to measured data that are already noisy. The effect of added noise on specimen mass, decay function $1 - E$, MEDEA spectra, and DEXFIT spectra are illustrated in Fig. 7 and Fig. S5 in the *Supplementary Material*. Five different Gaussian noise series were used in each case. The results show that random noise of this magnitude has a negligible effect on the obtained MEDEA and DEXFIT spectra.

Negative data

As moisture equilibrium is approached, $1 - E$ approaches zero. However, random noise in the data results in negative values of $1 - E$ towards the end of the sorption step. The software that was used to perform the MEDEA routine does not recognize negative values but instead treats them as positive values. To investigate how the presence of negative values of $1 - E$ affects MEDEA and DEXFIT spectra, we compared the original datasets with a dataset where all values of $1 - E$ were discarded from the first time point at which $1 - E$ was negative. The effect on the MEDEA spectra was found to be minor as seen in Fig. S6 in the *Supplementary Material*. In one case, removing negative values increased the number of DEXFIT components from four to five; this resulted in the DEXFIT spectrum more closely resembling the MEDEA spectrum.

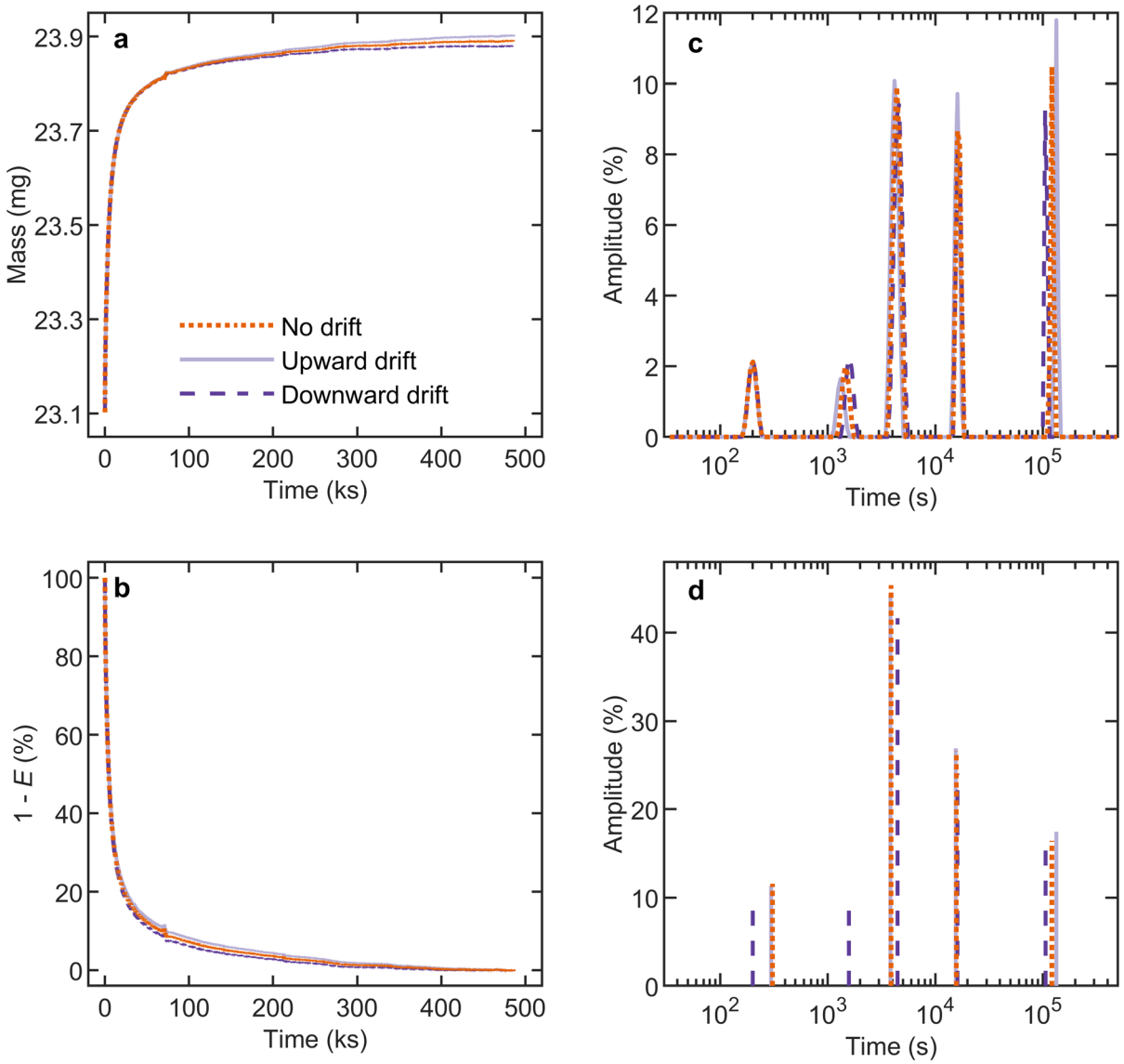

Fig. 6 Effect of simulated instrument drift on **a** specimen mass, **b** decay function $1 - E$, **c** MEDEA spectrum, and **d** DEXFIT spectrum for moisture absorption in loblolly pine from 70 to 80% RH

Erratic mass instability

The collection of sorption kinetic data over long times occasionally results in apparent sudden changes in specimen mass (bumps), e.g. due to vibrations affecting the instrument. Glass et al. (2017) used a simple additive correction to eliminate such bumps from the dataset. The effect of this on the MEDEA and DEXFIT spectra was investigated for a selection of absorption and desorption steps in holocellulose and loblolly pine. These steps were chosen to give a range in the magnitude of the bumps and the time of occurrence. Figure 8 illustrates an excessive example of a large bump in the desorption step 55–50% RH in holocellulose. Additional steps are documented in the *Supplementary Material* (Figs. S7–S9 and Tables S3–S4). The MEDEA spectra show a clear effect of correcting these bumps on both time constants and amplitude of the peaks. This suggests that mass stability is important in collecting sorption data. While these RH steps are included here to illustrate the effects on MEDEA and DEXFIT spectra,

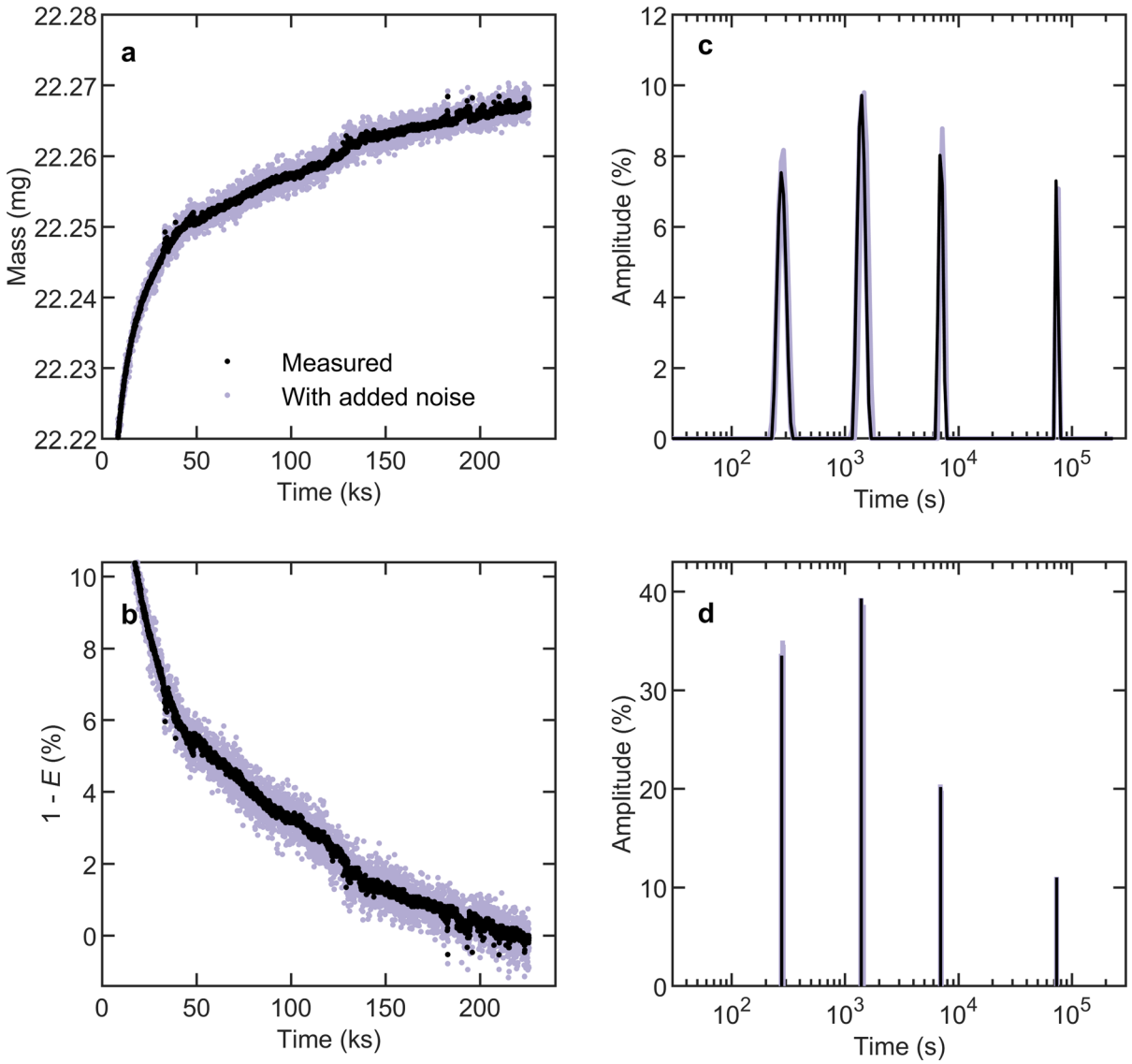

Fig. 7 Effect of simulated random noise on **a** specimen mass, **b** decay function $1 - E$, **c** MEDEA spectrum, and **d** DEXFIT spectrum for moisture absorption in loblolly pine from 20 to 30% RH. Simulated noise was Gaussian with a mean of 0 μg and standard deviation of 1 μg. A single noise profile is depicted in panels (**a**, **b**), and the vertical axes are scaled to show the magnitude of the noise at longer times. The spectra for five different noise profiles are plotted in panels (**c**, **d**)

in general data files that have significant mass instability should not be considered for further analysis.

Approach to equilibrium

The collection of sorption kinetic data lasted until the mass change was less than the inherent mass stability of the instrument. Consequently, the rate of water vapor sorption at the end of each step reached a level where the mass change it caused could not be distinguish from inherent instrument uncertainty. This resulted in measurements lasting 1.9–5.6 days (median: 2.9 days) in absorption steps and 3.0–15.2 days (median: 5.9 days) in desorption steps. While these measurement durations are much longer than those commonly reported in the literature for small specimens, the durations are still finite. Therefore, it is

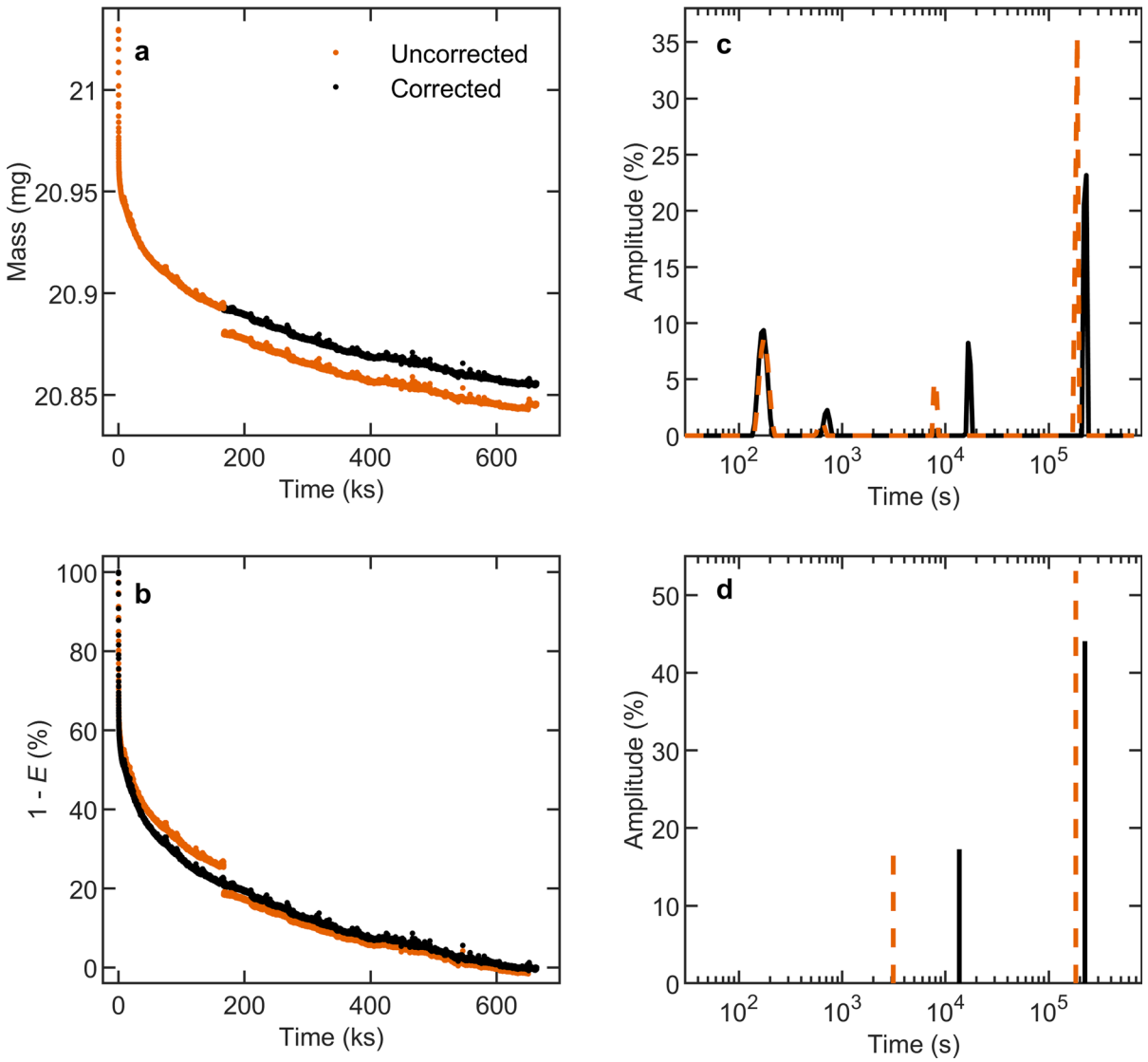

Fig. 8 Effect of erratic mass instability on **a** specimen mass, **b** decay function $1 - E$, **c** MEDEA spectrum, and **d** DEXFIT spectrum for moisture desorption in holocellulose from 55 to 50% RH

possible that considerably longer measurements would cause the mass to deviate from the one determined at the end of each sorption step. To investigate the effect of this slow approach to equilibrium, an arbitrary offset of 5% was added to the final mass, meaning that only 95% of the sorption process was assumed to be complete at the end of the step. This is illustrated in Fig. 9a, and the effect on $1 - E$ is shown in Fig. 9b. In the analysis of these data, the relaxation domain for MEDEA was assumed to extend 10 times longer than the last recorded time point to allow longer time constants to be determined. The results on the time constants can be seen in Fig. 9c, d. While similar time constants are found by MEDEA and DEXFIT, an additional exponential component appears with the 5% offset and the time values are shifted. Overall, one to three more exponentials are found for the sorption steps investigated (see Tables S5 and S6 in the *Supplementary Material)*, all of which can be resolved with respect to the resolution limit. Nonetheless, the overall distribution of relative weights of the individual exponentials remains, but the additional exponential highlights the importance of prolonged measurements to capture the

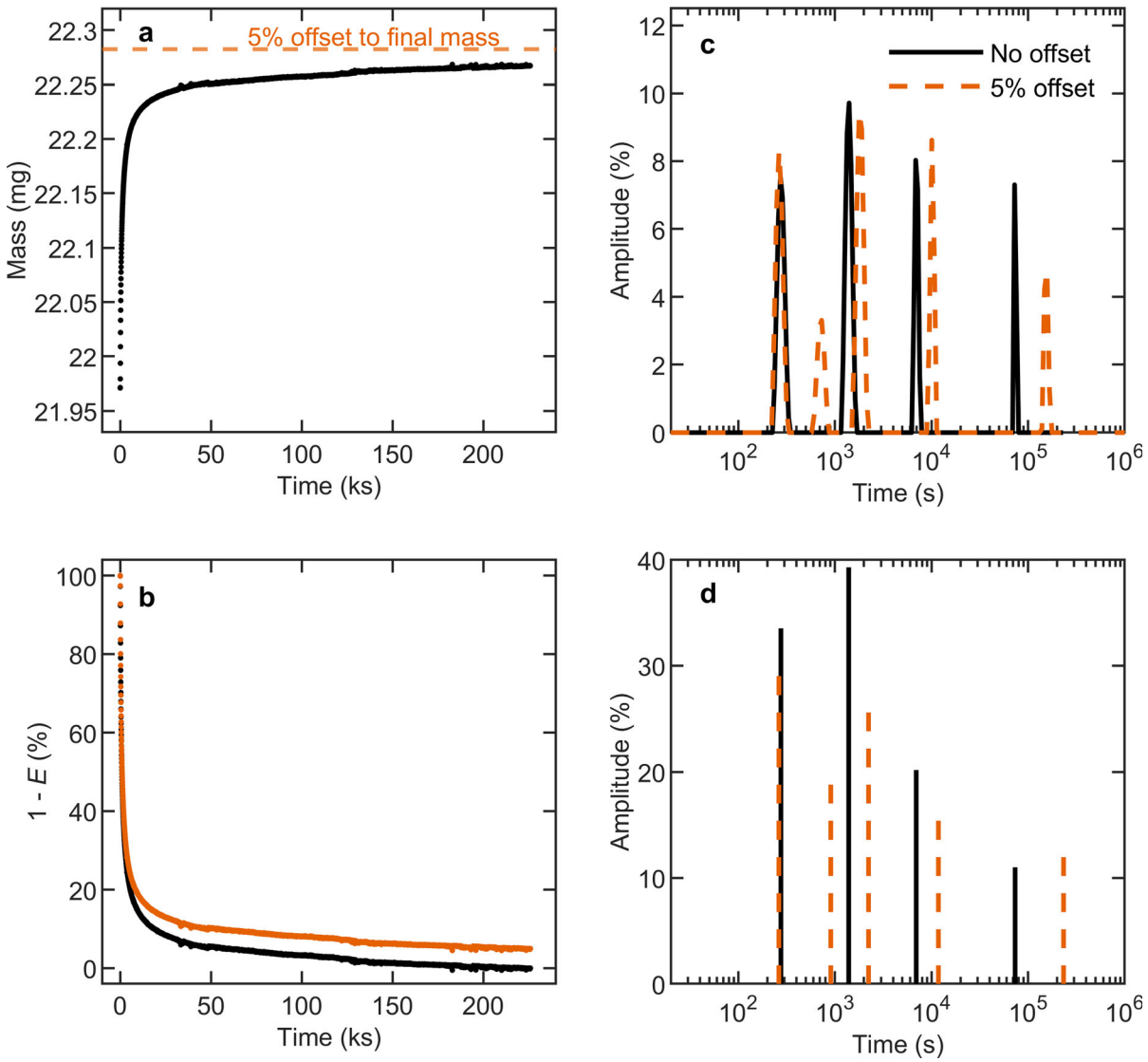

Fig. 9 Effect of a 5% offset from equilibrium in the final data point on **a** specimen mass, **b** decay function $1 - E$, and (**c**, **d**) MEDEA and DEXFIT spectra for moisture absorption in loblolly pine from 20 to 30% RH

dominant exponential components. While these results are based on a hypothetical mass offset, improving the instrument mass stability and further tightening the equilibrium criterion would reduce the uncertainty in the exponential decay analysis.

Applications of exponential decay analysis

All of the theoretical and empirical models in Table 1 describe sorption kinetic data as a sum of exponentials. They are, however, all constrained in either the number of exponential components or in the relationship between the individual pre-exponential coefficients and the respective time constants. Forcing either type of mathematical model onto sorption kinetic data may yield reasonable goodness of fit. However, this does not imply that the specific model can mathematically capture the actual form of the sorption curve, as discussed in the introduction. As illustrated in Figs. 3 and 4, exponential decay analysis with DEXFIT and MEDEA is a flexible, data-driven methodology that overcomes this problem. From these figures the appropriateness of the models in Table 1 can be directly evaluated from analysis of their

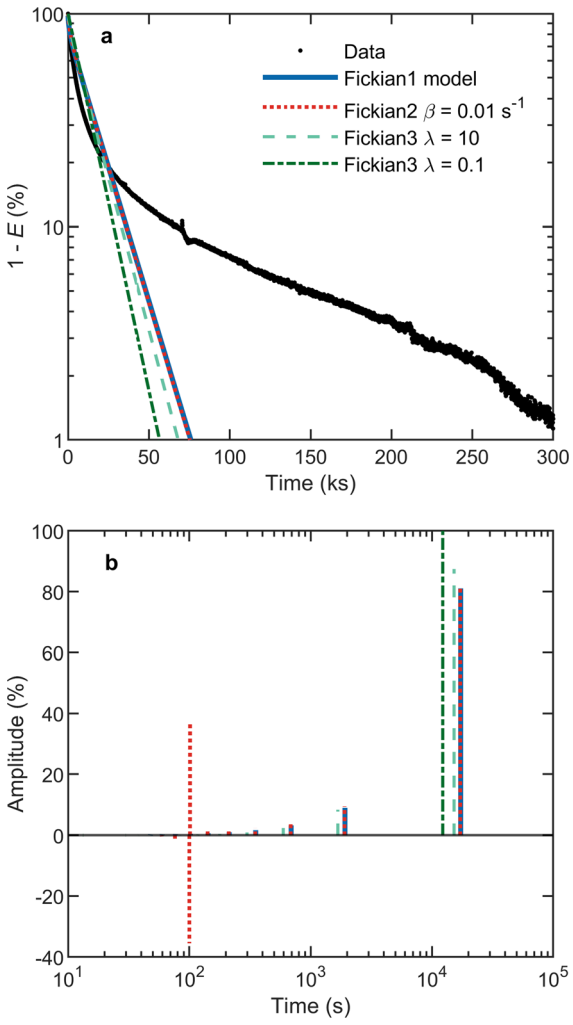

Fig. 10 Exponential fingerprints of the Fickian diffusion model with the three different boundary conditions. **a** Fit to data for loblolly pine in the 70–80% RH sorption step, and **b** exponential fingerprints of the three varieties of the Fickian diffusion model

"fingerprint". In this context, we use fingerprint to describe the number of exponentials, the relative magnitude of their peaks, and the peak spacing. For instance, none of the models with one or two exponential components (Lagergren, PEK, Sircar, and TLMT) can fit all sorption steps since at least one sorption step for all materials contain more than two exponential components. Similarly, the fingerprint of the Fickian diffusion model cannot be found in the results of Figs. 3 and 4 regardless of the boundary conditions. This is illustrated in Fig. 10, where the first 10 terms in the infinite sum of the 'Fickian1', 'Fickian2' and 'Fickian3' models are fitted to the sorption step 70–80% RH for loblolly pine (see *Supplementary Material* for further details). For the 'Fickian1' model, the amplitude diminishes rapidly going from the largest time constant ($\tau_1 = 1.7 \times 10^4$ s) to the smallest ($\tau_{10} = 48$ s). For the 'Fickian2' and 'Fickian3' models, the amplitudes and time constants depend on the values of β and λ, respectively. For the 'Fickian2' model that has the surface concentration changing over time with a time constant of β^{-1}, negative coefficients were sometimes observed which result in a lag-phase at early times. In Fig. 10 a significant negative coefficient is observed for the exponential with τ_1 which is, however, cancelled out by a positive coefficient of similar size for τ_8. The fingerprints of the three versions of the Fickian diffusion model shown in Fig. 10 are clearly different from the MEDEA and DEXFIT spectra for all the sorption steps plotted in Figs. 3 and 4. That is not to say that Fickian diffusion does not occur in the lignocellulosic materials investigated. However, it is evident from the DEXFIT and MEDEA results that Fickian diffusion alone cannot explain sorption kinetics. It is only the Berens–Hopfenberg model that in principle could describe the results of Figs. 3 and 4 by minimizing the Fickian contribution, i.e. setting φ_D close to zero, and selecting a variable number of exponential components to describe stress relaxation, i.e. tuning the parameter k to between 2 and 5 for each sorption step. This goes against the finding by Berens and Hopfenberg (1978), however, that only one or two components are needed to adequately describe the contribution from stress relaxation.

In general, Figs. 3 and 4 illustrate the complexity of water vapor sorption kinetics in lignocellulosic materials, where the number of exponential components needed to describe the data varies between the different materials, the relative humidity level, and even between absorption and desorption between the same levels of relative humidity for the same type of material. It should be noted, however, that the difference in the number of exponential components may be a result of two or more components having closely spaced time constants under certain conditions. Hereby, the methodology would only find one component if the spacing between the time constants of the components is less than the resolution limit determined by the signal-to-noise ratio in Eq. (3). This also highlights the need for good quality sorption kinetic data to resolve components with closely spaced

time constants. In this study, the signal-to-noise ratio of the sorption kinetic data ranges from 196 (office paper, 20–25% RH) to 2895 (holocellulose, 70–80% RH) which sets the resolution limit, δ, to 2.22 and 1.74, respectively. Improving the signal-to-noise by one order of magnitude would result in a resolution limit of 1.79 and 1.55, respectively.

The results in Figs. 3 and 4 clearly illustrate why previous attempts have failed in deriving meaning from fitting mathematical models to sorption kinetic data of lignocellulosic materials. The variability in the exponential behavior across materials, relative humidity levels, and sorption direction is undoubtedly a result of the complex interplay between multiple physical phenomena occurring during sorption (Thybring et al. 2019b). Finding the appropriate physical model that can adequately describe this behavior is challenging. Figures 3 and 4 illustrate the usefulness of exponential decay analysis in evaluating the appropriateness of theoretical and empirical models such as those in Table 1 in representing sorption kinetic data. Therefore, even though the methodology does not ascribe physical meaning to the fitting parameters derived by DEXFIT or MEDEA, it can be used to test any model that can be represented as a sum of exponential functions by comparing the model fingerprint with that of the data.

Conclusions

Exponential decay analysis on sorption kinetic data is a useful tool for examining the approach to moisture equilibrium in cellulosic materials. Unlike other methods that are constrained by a fixed number of fitting parameters or similar constraints, exponential decay analysis is a flexible, data-driven methodology for analyzing sorption kinetics. This approach does not assign physical significance to the exponential components a priori. The two different methodologies for exponential decay analysis employed in this study arrive at closely similar results for the dominant exponentials describing the examined sorption kinetic data. These exponentials are described by their characteristic time constants and their relative weights. The correspondence between the two methodologies underscores the robustness of exponential decay analysis, since these methodologies are based on two fundamentally different approaches: One fits the sum of a limited number of exponentials to the experimental data with freedom to vary both time constants and relative weights, while the other fits the sum of a large number of exponentials with predefined, logarithmically spaced time constants, with freedom to vary only the relative weights. The relative distribution of peaks provided by exponential decay analysis are shown to be robust in relation to instrument drift and noise. Therefore, the methodology provides a novel path to evaluate sorption kinetic data without prior knowledge. This is particularly useful in the current situation where models for properly describing the physics of sorption kinetics are still lacking. Exponential decay analysis performed by either DEXFIT or MEDEA offers a reliable description of the dominant time scales of sorption kinetics, which opens the way for the testing of new models. Combining exponential decay analysis with further experimental investigation and model development may lead to deeper understanding of physical mechanisms governing sorption kinetics.

Acknowledgments Funding was provided by the US Forest Service and the University of Copenhagen. On behalf of all authors, the corresponding author states that there is no conflict of interest.

References

Araujo CD, Mackay AL, Hailey JRT, Whittall KP, Le H (1992) Proton magnetic-resonance techniques for characterization of water in wood—application to white spruce. Wood Sci Technol 26:101–113. https://doi.org/10.1007/BF00194466

Barkas WW (1932) Retention of moisture by wood. Nature 130:699–700. https://doi.org/10.1038/130699c0

Beck G, Thybring EE, Thygesen LG, Hill C (2018) Characterization of moisture in acetylated and propionylated radiata pine using low-field nuclear magnetic resonance (LFNMR) relaxometry. Holzforschung 72:225. https://doi.org/10.1515/hf-2017-0072

Berens AR, Hopfenberg HB (1978) Diffusion and relaxation in glassy polymer powders: 2. Separation of diffusion and relaxation parameters. Polymer 19:489–496. https://doi.org/10.1016/0032-3861(78)90269-0

Bertero M, Boccacci P, Pike ER (1982) On the recovery and resolution of exponential relaxation rates from experimental data: a singular-value analysis of the Laplace transform inversion in the presence of noise. P Roy Soc A-Math Phys 383:15–29. https://doi.org/10.1098/rspa.1982.0117

Boyd GE, Adamson AW, Myers LS (1947) The exchange adsorption of ions from aqueous solutions by organic

zeolites. II Kinetics J Am Chem Soc 69:2836–2848. https://doi.org/10.1021/ja01203a066

Chihara K, Suzuki M, Kawazoe K (1976) Effect of heat generation on measurement of adsorption rate by gravimetric method. Chem Eng Sci 31:505–507. https://doi.org/10.1016/0009-2509(76)80037-1

Christensen GN, Kelsey KE (1959) The rate of sorption of water vapor by wood. Holz Roh Werkst 17:178–188. https://doi.org/10.1007/BF02608810

Crank J (1975) The mathematics of diffusion, 2nd edn. Clarendon Press, Oxford, UK, p 414

Engelsen SB, Bro R (2003) Powerslicing. J Magn Reson 163:192–197. https://doi.org/10.1016/S1090-7807(03)00125-3

Fredriksson M, Thygesen LG (2017) The states of water in Norway spruce (*Picea abies* (L.) Karst.) studied by low-field nuclear magnetic resonance (LFNMR) relaxometry: assignment of free-water populations based on quantitative wood anatomy. Holzforschung 71:77–90. https://doi.org/10.1515/hf-2016-0044

Glass SV, Zelinka SL, Johnson JA (2014) Investigation of historic equilibrium moisture content data from the Forest Products Laboratory. Forest Service, Forest Products Laboratory, General Technical Report, FPL-GTR-229, Madison, WI, USA, 35 pp. https://doi.org/10.2737/FPL-GTR-229

Glass SV, Boardman CR, Zelinka SL (2017) Short hold times in dynamic vapor sorption measurements mischaracterize the equilibrium moisture content of wood. Wood Sci Technol 51:243–260. https://doi.org/10.1007/s00226-016-0883-4

Glass SV, Boardman CR, Thybring EE, Zelinka SL (2018) Quantifying and reducing errors in equilibrium moisture content measurements with dynamic vapor sorption (DVS) experiments. Wood Sci Technol 52:909–927. https://doi.org/10.1007/s00226-018-1007-0

Glueckauf E, Coates JI (1947) 241. Theory of chromatography. Part IV. The influence of incomplete equilibrium on the front boundary of chromatograms and on the effectiveness of separation. J Chem Soc 1947:1315–1321. https://doi.org/10.1039/JR9470001315

Guo X, Wu Y, Xie X (2017) Water vapor sorption properties of cellulose nanocrystals and nanofibers using dynamic vapor sorption apparatus. Sci Rep 7:14207. https://doi.org/10.1038/s41598-017-14664-7

Hill CAS, Norton A, Newman G (2010) Analysis of the water vapour sorption behaviour of Sitka spruce [*Picea sitchensis* (Bongard) Carr.] based on the parallel exponential kinetics model. Holzforschung 64:469–473. https://doi.org/10.1515/hf.2010.059

Himmel S, Mai C (2016) Water vapour sorption of wood modified by acetylation and formalisation—analysed by a sorption kinetics model and thermodynamic considerations. Holzforschung 70:203–213. https://doi.org/10.1515/hf-2015-0015

Istratov AA, Vyvenko OF (1999) Exponential analysis in physical phenomena. Rev Sci Instrum 70:1233–1257. https://doi.org/10.1063/1.1149581

Jalaludin Z, Hill CAS, Samsi HW, Husain H, Xie Y (2010) Analysis of water vapour sorption of oleo-thermal modified wood of *Acacia mangium* and *Endospermum malaccense* by a parallel exponential kinetics model and according to the Hailwood-Horrobin model. Holzforschung 64:763–770. https://doi.org/10.1515/hf.2010.100

Kohler R, Dück R, Ausperger B, Alex R (2003) A numeric model for the kinetics of water vapor sorption on cellulosic reinforcement fibers. Compos Interface 10:255–276. https://doi.org/10.1163/156855403765826900

Krabbenhøft K, Damkilde L (2004) A model for non-Fickian moisture transfer in wood. Mater Struct 37:615–622. https://doi.org/10.1007/BF02483291

Lagergren S (1898) Zur Theorie der sogenannten Adsorption gelöster Stoffe [On the theory of so-called adsorption of soluble substances]. Kungliga Svenska Vetenskapsakademiens Handlingar 24:1–39

Lawson CA, Hanson R (1974) Linear least squares with linear inequality constraints solving east squares problems. Prentice-Hall, Englewood Cliffs, USA, pp 158–173

Lee L-K, Ruthven DM (1979) Analysis of thermal effects in adsorption rate measurements. J Chem Soc Faraday T1(75):2406–2422. https://doi.org/10.1039/F19797502406

McWhirter JG, Pike ER (1978) On the numerical inversion of the Laplace transform and similar Fredholm integral equations of the first kind. J Phys A-Math Gen 11:1729–1745. https://doi.org/10.1088/0305-4470/11/9/007

Murr A, Lackner R (2018) Analysis on the influence of grain size and grain layer thickness on the sorption kinetics of grained wood at low relative humidity with the use of water vapour sorption experiments. Wood Sci Technol 52:753–776. https://doi.org/10.1007/s00226-018-1003-4

Olek W, Perré P, Weres J (2005) Inverse analysis of the transient bound water diffusion in wood. Holzforschung 59:38–45. https://doi.org/10.1515/HF.2005.007

Ostrowsky N, Sornette D, Parker P, Pike ER (1981) Exponential sampling method for light scattering polydispersity analysis. Opt Acta 28:1059–1070. https://doi.org/10.1080/713820704

Pedersen HT, Bro R, Engelsen SB (2002) Towards rapid and unique curve resolution of low-field NMR relaxation data: trilinear SLICING versus two-dimensional curve fitting. J Magn Reson 157:141–155. https://doi.org/10.1006/jmre.2002.2570

Pidgeon LM, Maass O (1930) The adsorption of water by wood. J Am Chem Soc 52:1053–1069. https://doi.org/10.1021/ja01366a033

Sheppard SE, Newsome PT (1929) The sorption of water vapor by cellulose and its derivatives. J Phys Chem 33:1817–1835. https://doi.org/10.1021/j150305a015

Sheppard SE, Newsome PT (1930) The sorption of water vapor by cellulose and derivatives Part II The kinetics of sorption. J Phys Chem 34:1158–1165. https://doi.org/10.1021/j150312a003

Simón C, Esteban LG, Palacios PD, Fernández FG, García-Iruela A (2017) Sorption/desorption hysteresis revisited. Sorption properties of *Pinus pinea* L analysed by the parallel exponential kinetics and Kelvin–Voigt models. Holzforschung 71:171. https://doi.org/10.1515/hf-2016-0097

Sircar S (1983) Linear-driving-force model for non-isothermal gas adsorption kinetics. J Chem Soc Faraday T1(79):785–796. https://doi.org/10.1039/F19837900785

Thybring EE, Boardman CR, Glass SV, Zelinka SL (2019a) The parallel exponential kinetics model is unfit to characterize moisture sorption kinetics in cellulosic materials. Cellulose 26:723–735. https://doi.org/10.1007/s10570-018-2134-3

Thybring EE, Glass SV, Zelinka SL (2019b) Kinetics of water vapor sorption in wood cell walls: state of the art and research needs. Forests 10:704. https://doi.org/10.3390/f10080704

Thybring EE, Kymäläinen M, Rautkari L (2018) Experimental techniques for characterising water in wood covering the range from dry to fully water-saturated. Wood Sci Technol 52:297–329. https://doi.org/10.1007/s00226-017-0977-7

Tiemann HD (1906) Effect of moisture upon the strength and stiffness of wood vol Bulletin 70. US Department of Agriculture, Forest Service, Washington, DC, USA

Urquhart AR (1929) The mechanism of the adsorption of water by cotton. J Text Inst 20:T125–T132. https://doi.org/10.1080/19447022908661485

Urquhart AR, Williams AM (1924) A review of work on the absorption and desorption of moisture by textile materials. T Faraday Soc 20:0309–0313. https://doi.org/10.1039/TF9242000309

Volbehr BFKJ (1896) Untersuchungen über die Quellung der Holzfaser [Investigations of the swelling of wood fibres]. Ph.D. thesis, Kiel University, Germany, 37 pp

Wadsö L (1993) Measurements of water–vapor sorption in wood.2. Results Wood Sci Technol 28:59–65. https://doi.org/10.1007/BF00193877

Wang P, Meldon JH, Sung N (1996) Heat effects in sorption of organic vapors in rubbery polymers. J Appl Polym Sci 59:937–944. https://doi.org/10.1002/(sici)1097-4628(19960207)59:6%3c937::aid-app5%3e3.0.co;2-q

Wilczak A, Keinath TM (1993) Kinetics of sorption and desorption of copper(II) and lead(II) on activated carbon. Water Environ Res 65:238–244. https://doi.org/10.2175/WER.65.3.7

Willems W (2017) Thermally limited wood moisture changes: relevance for dynamic vapour sorption experiments. Wood Sci Technol 51:751–770. https://doi.org/10.1007/s00226-017-0905-x

Xie YJ, Hill CAS, Jalaludin Z, Curling SF, Anandjiwala RD, Norton AJ, Newman G (2011) The dynamic water vapour sorption behaviour of natural fibres and kinetic analysis using the parallel exponential kinetics model. J Mater Sci 46:479–489. https://doi.org/10.1007/s10853-010-4935-0

Zaihan J, Hill CAS, Curling S, Hashim WS, Hamdan H (2010) The kinetics of water vapour sorption: analysis using parallel exponential kinetics model on six Malaysian hardwoods. J Trop For Sci 22:107–117